scientific reports

Check for updates

OPEN

Metabolomic analysis of the intrinsic resistance mechanisms of *Microtus fortis* against *Schistosoma japonicum* infection

Tianqiong He[1,2], Du Zhang[3,4], Yixin Wen[1,2], Qian Liu[1,2], Junkang Zhou[1,2], Wenling Zhi[1,2], Lingxuan OuYang[1,2], Yushan Qi[1,2], Zikang Zhou[1,2], Xin Gao[1,2], Fan Li[1,2], Zhijie Su[1,2], Jia Shen[5,6,7] & Zhijun Zhou[1,2]✉

Microtus fortis **(*M. fortis*) is the only mammal known in China that is intrinsically resistant to *Schistosoma japonicum* (*S. japonicum*) infection. Nevertheless, the underlying resistance mechanism of *M. fortis* against schistosomes are still unclear. In this study, we detected and compared colon aqueous extracts and serum metabolic profiles between *M. fortis* and ICR mice before and after *S. japonicum* infection using liquid chromatography–mass spectrometry (LC–MS). We identified 232 specific colon aqueous extract metabolites and 79 specific serum metabolites of *M. fortis* infected with or without *S. japonicum* at two weeks compared with those of ICR mice, which might be closely correlated with the time-course of schistosomiasis progression and could also be used as indicators for the *M. fortis* against *S. japonicum*, for example, nonadecanoic acid, hesperetin, glycocholic acid, 2-Aminobenzoic acid, 6-hydroxydaidzein and spermidine. And the enriched pathways were further identified, our findings revealed that *S. japonicum* infection induced the metabolic changes involved in a variety of metabolic pathways including amino acid metabolism, lipid metabolism, ABC transporters, central carbon metabolism in cancer and bile secretion. These results indicated that the colon aqueous extracts and serum metabolic profiles were significantly different between *M. fortis* and ICR mice before and after *S. japonicum* infection and will provide new insights into the underlying resistance mechanism of *M. fortis* against *S. japonicum* infection and identify promising candidates for the use of drugs against schistosomes.**

Keywords Metabolomics, Serum, Colon aqueous extracts, *Schistosoma japonicum*, *M. fortis*, ICR mice, Intrinsic resistance mechanism

Schistosomiasis, also known as bilharzia, is an acute and chronic parasitic disease caused by blood flukes of the genus *Schistosoma*, with over 250 million people infected and approximately 200,000 deaths annually[1,2]. The three major schistosome species infecting humans are *Schistosoma mansoni* (*S. mansoni*), *Schistosoma hematobium* (*S. hematobium*), and *Schistosoma japonicum* (*S. japonicum*), among which *S. japonicum* produces the greatest number of eggs and is the most prevalent in China, Indonesia, and the Philippines[3]. Moreover, schistosomes have a complicated life cycle involving both asexual reproduction in intermediate hosts (snails) and sexual reproduction in definitive hosts (mammals)[4]. The cercariae penetrate the skin and shed their forked tails in suitable mammalian hosts for infection, forming schistosomula[5]. Schistosomula travel through the lungs and heart, develop in the liver, and finally mature in the mesenteric veins (*S. mansoni*, *S. japonicum*) or perivesical veins (*S. hematobium*)[6].

[1]Department of Laboratory Animal Science, Xiangya Medical College, Changsha 410013, Hunan, China. [2]Hunan Key Laboratory of Animal Models for Human Diseases, Central South University, Changsha 410013, Hunan, China. [3]Department of Medical Genetics, The Second Xiangya Hospital, Central South University, Changsha 410011, China. [4]Hunan Province Clinical Medical Research Center for Genetic Birth Defects and Rare Diseases, Department of Medical Genetics, The Second Xiangya Hospital, Central South University, Changsha 410011, China. [5]Department of Parasitology, Zhongshan School of Medicine, Sun Yat-Sen University, Guangzhou 510080, Guangdong, China. [6]Key Laboratory of Tropical Disease Control of the Ministry of Education, Sun Yat-sen University, Guangzhou 510080, Guangdong, China. [7]Provincial Engineering Technology Research Center for Biological Vector Control, Guangzhou 510080, Guangdong, China. ✉email: zhouzhijun@csu.edu.cn

Microtus fortis (*M. fortis*), also known as reed voles, is the only mammalian host that has exhibited intrinsic resistance against *S. japonicum* infection[7,8]. This resistance can be inherited and is not affected by geographical distribution or environmental change[9]. Cercariae invade via the skin and migrate through the lungs to the liver in *M. fortis* eventually. Still, the development of *S. japonicum* in *M. fortis* is arrested on day 12 after infection. And the worms gradually become atrophied and ultimately die in the liver by 3–4 weeks after infection, resulting in the parasites not completing their life cycle[10]. However, *S. japonicum* grow to become mature, mate, and produce eggs in mice, which is a permissive host of *S. japonicum*. The schistosomula migrate to the lungs within 3–5 days and then to the hepatic portal system at approximately 14 days post infection (p.i.). The schistosomes in copula migrate to the mesenteric veins (*S. mansoni* and *S. japonicum*) and release their eggs into the tissue after approximately 28 days p.i[11]. To date, many studies have reported the intrinsic resistance mechanism of *M. fortis* against schistosome infection. For example, the serum components complement, antibodies, albumin, immune response, and some effector molecules of *M. fortis* are involved in resistance mechanisms[9,12,13]. However, the underlying molecular mechanisms of this resistance are not yet known.

Metabolomics is a powerful tool for studying the host metabolic response to parasitic infection[14,15]. As the substrates and products of metabolism, metabolites drive essential cellular functions, such as energy production and storage, signal transduction, and immunological adaptation[16]. Additionally, LC-MS-based metabolomics analysis revealed that energy metabolism, immune responses, glucose uptake and metabolism, amino acid metabolism, DNA and RNA biosynthesis, and gut microbiota metabolism pathways were disrupted in mice infected with *S. japonicum*, and some specific metabolites were significantly downregulated and closely correlated with the time course of schistosomiasis progression[17]. Therefore, metabolomics could provide novel insights into the mechanisms underlying the progression of schistosomiasis and the resistance mechanism between the host and *S. japonicum*. For example, previous studies have assessed that the liver metabolism of *M. fortis* before or after infection with *S. japonicum* at two weeks, which is the peak time for *M. fortis* to clear schistosome, and these results found 25 different metabolites between the uninfected and infected *M. fortis*[8,10]. Even through the *S. japonicum* do not eventually enter the gut of *M. fortis*, increasing evidence suggests that the gut microbiome influences the progression of schistosomiasis and plays a central role in liver disease via the gut-liver axis[18]. The glossary "gut-liver axis" was proposed to emphasize the substantial interactions between gut and host liver. The gut metabolites may have resistance effects on the host liver through the gut-liver axis, improving the physical immunity and further contributing to the natural resistance to *S. japonicum*. Besides, our previous reports the remarkable alterations of *M. fortis* colonic microbiota in both community structure and potential functions along with the resistance to *S. japonicum* infection[19]. Therefore, we performed a comprehensive LC-MS-based metabolomics analysis of colon aqueous extracts and serum samples from *M. fortis* and ICR mice infected with or without by *S. japonicum* at two weeks, and further identified the differentially abundant metabolites and enriched pathways. Finally, this study aimed to explore the role of host metabolomics in elucidating the intrinsic resistance mechanism of *M. fortis* against *S. japonicum* infection, to provide new insights into host-parasite interactions from systematic and metabolic perspectives, and to pave the way for the development of drugs to treat schistosomiasis.

Materials and methods

Ethics statement

This animal study was conducted in the light of the standards of the Laboratory of Animal Welfare & Ethics Committee of China strictly. And the protocol was approved by the Laboratory Animal Welfare and Ethics Committee of Central South University (Changsha, China; approval no. CSU-2022-0654). All methods were carried out in accordance with relevant guidelines and regulations. This study was conducted as recommended by the ARRIVE guidelines.

Animals and parasites

M. fortis from the Dongting Lakes region and ICR mice were purchased from Hunan Silaike Jingda Laboratory Animal Co., Ltd., and all animals were housed at Xiangya Medical College, Central South University (Changsha, China), as previously described[20]. *S. japonicum* cercariae was obtained from infected *Oncomelania hupensis* snails provided by the Jiangsu Institute of Parasitic Diseases (Wuxi, China). The infected snails were placed in dechlorinated water under artificial light to induce cercarial shedding before animal infection[21]. Totally 10 male *M. fortis* (weighting 40–60 g) and 10 male ICR mice (weighting 20–30 g), approximately 8 weeks old, were randomly divided into two groups: a control group (uninfected group), infected group at two weeks, with 5 *M. fortis* and 5 ICR mice in each group. *M. fortis* was infected with 100 cercariae, and ICR mice were infected with 20 cercariae in two infected groups, respectively. Animals with significant weight differences and schistosome infection unsuccessfully, including the negative pathological results detected by HE staining, or the number of infected worms varies greatly were excluded. The sample sizes were selected based on previous experience and published literature.

Sample collection and preparation

All animals were anesthetised using 3% isoflurane and kept under anesthesia using 2-3% isoflurane during the entire infection procedure, where the abdominal cavity was opened. The portal vein was found and the portal vein blood was collected with the use of a 1-mL syringe. The colon was found and then the colonic contents was collected at frozen pipes, then the colon was discarded. The liver was isolated carefully and fixed with 4% paraformaldehyde for histopathological examination. Colonic contents, blood from the portal vein and liver tissue were collected at 0 and 2 weeks after infection, respectively. Then, the colonic contents were added MeOH and glass bead in turn, grinded, ultrasound, centrifuged, and filtered to prepare the colon aqueous extracts for LC-MS detection, respectively[22]. And the blood samples were centrifuged at 4,000 rpm for 15 min to obtain

serum at 4 °C, mixed, transferred into a 2 mL centrifuge tube, and then add 400 µL methanol (stored at -20 °C) and 2-chloro-l-phenylalanine (4 ppm) solution prepared with 80% methanol water (stored at 4 °C) in turn to prepare the samples for LC-MS detection[17]. Finally, the samples were processed for liquid chromatography and mass spectrometry (LC-MS) analysis with methanol and acetonitrile as previously described[23]. And all animals in each group were euthanized by CO_2 inhalation either before infection or at 2 weeks post-infection. Because a few serum samples failed the quality test, serum samples of four infected *M. fortis*, four control ICR mice, and four infected ICR mice were used for data analysis finally. We conducted a double-blind, randomized control trial in our study. On the one hand, the animal grouping in experimental and control groups was blinded. On the other hand, the trial was conducted twice, and the experimenters were different and blinded. The objectivity of the trial evaluation was ensured based on the double-blind methods.

Histological analysis

The liver tissue samples were fixed in 4% paraformaldehyde, and then dehydrated, embedded in paraffin, cut into 4-µm-thick sections, and mounted on glass slides. Next, the tissue samples were stained with H&E according to the standard procedures. Pathological changes in the morphology of cells were observed under a light microscope.

LC–MS conditions

Ultrahigh-performance liquid chromatography (UHPLC) analysis was performed on a Thermo Vanquish system (Thermo Fisher Scientific, USA). An ACQUITY UPLC® HSS T3 (150 × 2.1 mm, 1.8 µm, Waters, Milford, MA, USA) was maintained at 40 °C and used to perform chromatographic separations. The flow rate and injection volume were set at 0.25 mL/min and 2 µL, respectively. For LC-ESI (+)-MS analysis, the mobile phase consisted of B2, 0.1% formic acid in acetonitrile (v/v), and A2, 0.1% formic acid in water (v/v). The gradient program was as follows: 2% B2 at 0–1 min, 2-50% B2 at 1–9 min, 50-98% B2 at 9–12 min, 98% B2 at 12–13.5 min, 98%-2% B2 at 13.5–14 min, and 2% B2 at 14–20 min. For LC-ESI (-)-MS analysis, the analytes were analyzed with (B3) acetonitrile and (A3) ammonium formate (5 mM). Separation was conducted under the following gradient: 2% B3 at 0–1 min, 2-50% B3 at 1–9 min, 50-98% B3 at 9–12 min, 98% B3 at 12–13.5 min, 98%-2% B3 at 13.5–14 min, and 2% B3 at 14–17 min.

Mass spectrometry was performed on a Q-exacting instrument (Thermo Fisher Scientific, USA) with an electrospray ionization (ESI) source. The data were collected using both positive and negative ion modes. The parameters were as follows: sheath gas pressure at 30 arb, aux gas flow at 10 arb, spray voltage set at 3.50 kV and − 2.50 kV for ESI (+) and ESI (-), respectively, capillary temperature set at 325 °C, MS1 range from mass/charge (m/z) 100 to 1000, and normalized collision energy set at 30 eV. At the same time, dynamic exclusion is used to remove unnecessary MS/MS information (20) automatically.

Data analysis

The raw data were processed using XCMS for peak alignment, feature detection, and retention time correction[24]. The normalized data of colon aqueous extracts sets contained 22,015 features (12619 features in ESI + mode and 9396 features in ESI- mode), and the normalized data of serum sets contained 27,609 features (13565 features in ESI + mode and 14044 features in ESI- mode). The metabolites were identified by accuracy mass (< 30 ppm) and MS/MS data, which were matched with HMDB[25] (http://www.hmdb.ca), massbank[26] (http://www.massbank.jp/), LipidMaps[27] (http://www.lipidmaps.org), mzcloud[28] (https://www.mzcloud.org) and KEGG[29,30] (http://www.genome.jp/kegg/). Robust LOESS signal correction (QC-RLSC) was applied for data normalization to correct for any systematic bias[31]. Data scaling was implemented using quality control samples (QC) based on the R package: MetNormalizer. After normalization, only ion peaks with relative standard deviations (RSDs) less than 30% in the QC were retained to ensure proper metabolite identification. After scaling the data, models were built via principal component analysis (PCA), orthogonal partial least-square discriminant analysis (OPLS-DA), and partial least-square discriminant analysis (PLS-DA). The metabolic profiles could be visualized as a score plot, where each point represents a sample. The corresponding loading plot and S-plot were generated to provide information on the metabolites that influence the clustering of the samples. All the models evaluated were tested for overfitting with 100-time permutation tests. The descriptive performance of the models was determined by R2 (cumulative) (perfect model: R2 (cum) = 1) values while their prediction performance was measured by Q2 (cumulative) (perfect model: Q2 (cum) = 1) and a permutation test. The permuted model should not be able to predict classes: R2 and Q2 values at the Y-axis intercept must be lower than those of Q2 and the R2 of the non-permuted model. OPLS-DA allowed the determination of discriminating metabolites using the variable importance on projection. The *P*-value, variable importance projection (VIP) produced by OPLS-DA, and fold change (FC) were applied to discover the variables contributing to the classification. Finally, one-way ANOVA was performed to reveal the significant differences in the variation among the control and infected groups. Differences were considered significant when $P < 0.05$, VIP > 1, and FC ≥ 1.2 or ≤ 0.8.

Pathway analysis

Differentially abundant metabolites were subjected to pathway analysis by MetaboAnalyst[32]. The metabolites identified via metabolomics were mapped to KEGG pathways for biological interpretation of higher-level systemic functions. The metabolites and corresponding pathways were visualized using the KEGG Mapper tool.

Results

System stability assessment

The results of HE staining showed that we successfully established a model of *S. japonicum* infection in *M. fortis* and ICR mice (Figure S1 C-D), demonstrating granulomatous inflammatory responses caused by the presence

of worms in the liver of the infected animals. Further, all the ion chromatograms of the QC samples exhibited stable retention times without obvious peak drifts in both ESI modes, which indicated the good capability of the LC-MS/MS-based metabolomics approach used in this study. The stability and reproducibility of the established method were evaluated by performing PCA on all the samples, and the QC samples were tightly clustered in PCA score plots (Fig. 1), which demonstrated the good stability and high reproducibility of the instrument.

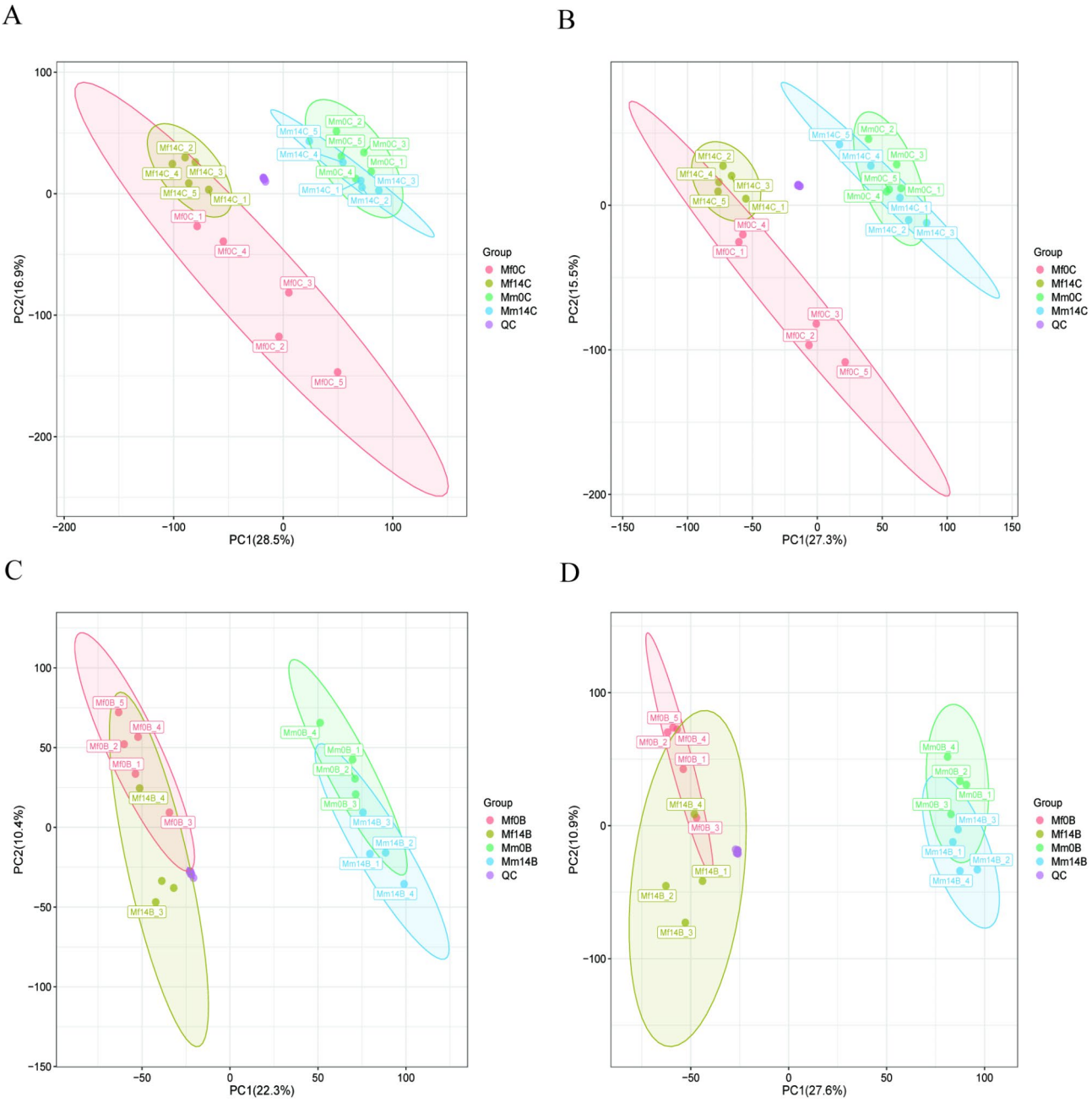

Fig. 1. Principal component analysis (PCA) score scatter plots of test samples and QC samples obtained from LC-MS/MS fingerprints in ESI + and ESI- modes. (**A**) Colon aqueous extracts samples in ESI + mode. (**B**) Colon aqueous extracts samples in ESI- mode. (**C**) Serum samples in ESI + mode. (**D**) Serum samples in ESI- mode. Mf0C: Colon aqueous extract samples of *M. fortis* without infection group; Mf14C: Colon aqueous extract samples of *M. fortis* after infection for 2 weeks; Mm0C: Colon aqueous extract samples of ICR mice without infection group; Mm14C: Colon aqueous extract samples of ICR mice after infection for 2 weeks; Mf0B: Serum samples of *M. fortis* without infection group; Mf14B: Serum samples of *M. fortis* after infection for 2 weeks; Mm0B: Serum samples of ICR mice without infection group; Mm14B: Serum samples of ICR mice after infection for 2 weeks.

Multivariate statistical analysis of colon aqueous extracts and serum metabolic profiles

To enhance the separation among the different groups, the supervised method PLS-DA was used. As shown in Fig. 2A, good separations were obtained between the aqueous colon extract samples from the infected *M. fortis* and infected ICR mice with or without *S. japonicum*, and between the uninfected and infected *M. fortis* (Fig. 2B), between the uninfected and infected ICR mice (Fig. 2C). For serum samples, obvious separations were achieved between the infected *M. fortis* and infected ICR mice with or without *S. japonicum* (Fig. 2D), between the infected and uninfected *M. fortis* (Fig. 2E) and between the infected and uninfected ICR mice (Fig. 2F). The permutation test results were shown in Supplementary Figure S4 reflected the data stability and the good fit.

Differential colon aqueous extracts and serum metabolic responses to *S. japonicum* infection in *M. fortis*

OPLS-DA on colon aqueous extract and serum samples yielded good separations of *M. fortis* infected with or without *S. japonicum* (Fig. 3A–B), and the S-plots obtained from OPLS-DA, were used to determine the meaningful and reliable variables that were attributed to the separation between the two groups (Supplementary Figure S2). The permutation test results of OPLS-DA models reflected the data stability and the good fit (Supplementary Figure S5 A-B). Furthermore, a total of 251 differentially abundant metabolites in the colon aqueous extracts were identified in *M. fortis* at two weeks p.i. compared with uninfected *M. fortis* (Fig. 3C, Supplementary Table 1). 223 of which showed an increasing trend, including hesperetin, glycocholic acid and N-Acetylneuraminic acid, and the remaining 28 metabolites showed a decreasing trend, i.e. myriocin, D-allo-isoleucine, cholestenone. In addition, 78 variables were identified in the serum of *M. fortis* at two weeks p.i. compared with those in the serum of uninfected *M. fortis* (Fig. 3D, Supplementary Table 2), and 22 of which showed an increasing trend, including neohesperidin, s-Lactoylglutathione, maltotriose and mitragynine, and the remaining 56 metabolites showed a decreasing trend, for example, genistein, allopurinol, ribose 1,5-bisphosphate were the top three decreasing terms. These findings indicated that *S. japonicum* infection disturbed normal biological processes in *M. fortis*.

Differential colon aqueous extracts and serum metabolic responses to *S. japonicum* infection in ICR mice

As showed in Fig. 4A-B, OPLS-DA also yielded good separation of ICR mice infected with or without *S. japonicum* at two weeks, and the S-plots are shown in Figure S2. The permutation test results of OPLS-DA models reflected the good fit (Supplementary Figure S5C,D).108 differentially abundant metabolites were identified in the colon aqueous extracts of infected ICR mice (Fig. 4C, Supplementary Table 3), 35 of which were increased significantly, i.e. prostaglandin F3a, 13,16,19-Docosatrienoic acid and N-Acetylneuraminic acid were the top three increasing terms, and 73 metabolites were decreasing significantly, for example, pyridoxamine 5'-phosphate, sedoheptulose, N6, N6-Dimethyladenosine were the top three decreasing terms. For serum, 51 differential metabolites were identified in ICR mice with or without *S. japonicum* infection (Fig. 4D, Supplementary Table 4), 11 of which showed an increasing trend, including sarsasapogenin, leukotriene D4 and antibiotic JI-20 A, and the remaining 40 metabolites showed a decreasing trend, such as beta-Sitosterol, 5-Hydroxyindoleacetylglycine, glycochenodeoxycholic acid.

Identification of differential colon aqueous extract metabolites for *S. japonicum* infection between *M. fortis* and ICR mice

OPLS-DA also yielded good separations between uninfected *M. fortis* and uninfected ICR mice (Fig. 5A), as well as infected *M. fortis* and infected ICR mice (Fig. 5B), and the S-plots are shown in Figure S2. The permutation test results of OPLS-DA models reflected the good fit (Supplementary Figure S5 E-F). The 271 most important colon aqueous extract metabolites (114 upregulated and 157 downregulated) were identified between the uninfected *M. fortis* and ICR mice (Fig. 5C, Supplementary Table 5). In addition, 370 differential colon aqueous extract metabolites (285 upregulated and 85 downregulated) were selected between the infected *M. fortis* and ICR mice with *S. japonicum* at two weeks (Fig. 5D, Supplementary Table 6). Venn analysis revealed 232 specific differentially abundant metabolites in *M. fortis* at two weeks after infection (194 upregulated and 38 downregulated) (Fig. 5E; Supplementary Table S9). Noticeably, the nonadecanoic acid (FC = 90.9), hesperetin (FC = 41.8) and glycocholic acid (FC = 40.4) were the top three increased terms specially in infected *M. fortis*. And "carboxylic acids and derivatives" was the most enriched metabolic terms of the differentially abundant metabolites of infected *M. fortis* (Fig. 5F). These results showed that there were significant differences in the metabolic profiles of the colon aqueous extracts between *M. fortis* and ICR mice after *S. japonicum* infection.

Identification of differential serum metabolites for *S. japonicum* infection between *M. fortis* and ICR Mice

OPLS-DA yielded good separations between *M. fortis* and ICR mice infected with or without *S. japonicum* (Fig. 6A,B), and the S-plots are shown in Figure S2. The permutation test results of OPLS-DA models reflected the good fit (Supplementary Figure S5 G-H). Moreover, 133 differential serum metabolites (84 upregulated and 49 downregulated) were detected between uninfected *M. fortis* and ICR mice (Fig. 6C, Supplementary Table 7). Additionally, 130 differential serum metabolites in *M. fortis* at two weeks after infection, 92 of which showed a significant increasing trend and the remaining 38 metabolites showed a decreasing trend in infected *M. fortis* (Fig. 6D, Supplementary Table 8). Moreover, venn analysis revealed 79 specific serum metabolites in *M. fortis* at two weeks after infection (53 upregulated and 26 downregulated) (Fig. 6E; Supplementary Table S10). And the 2-aminobenzoic acid (FC = 229.87), 6-hydroxydaidzein (FC = 113.94) and spermidine (FC = 92.04) were the top three increased terms specially in infected *M. fortis*. In addition, metabolite classification analysis revealed that

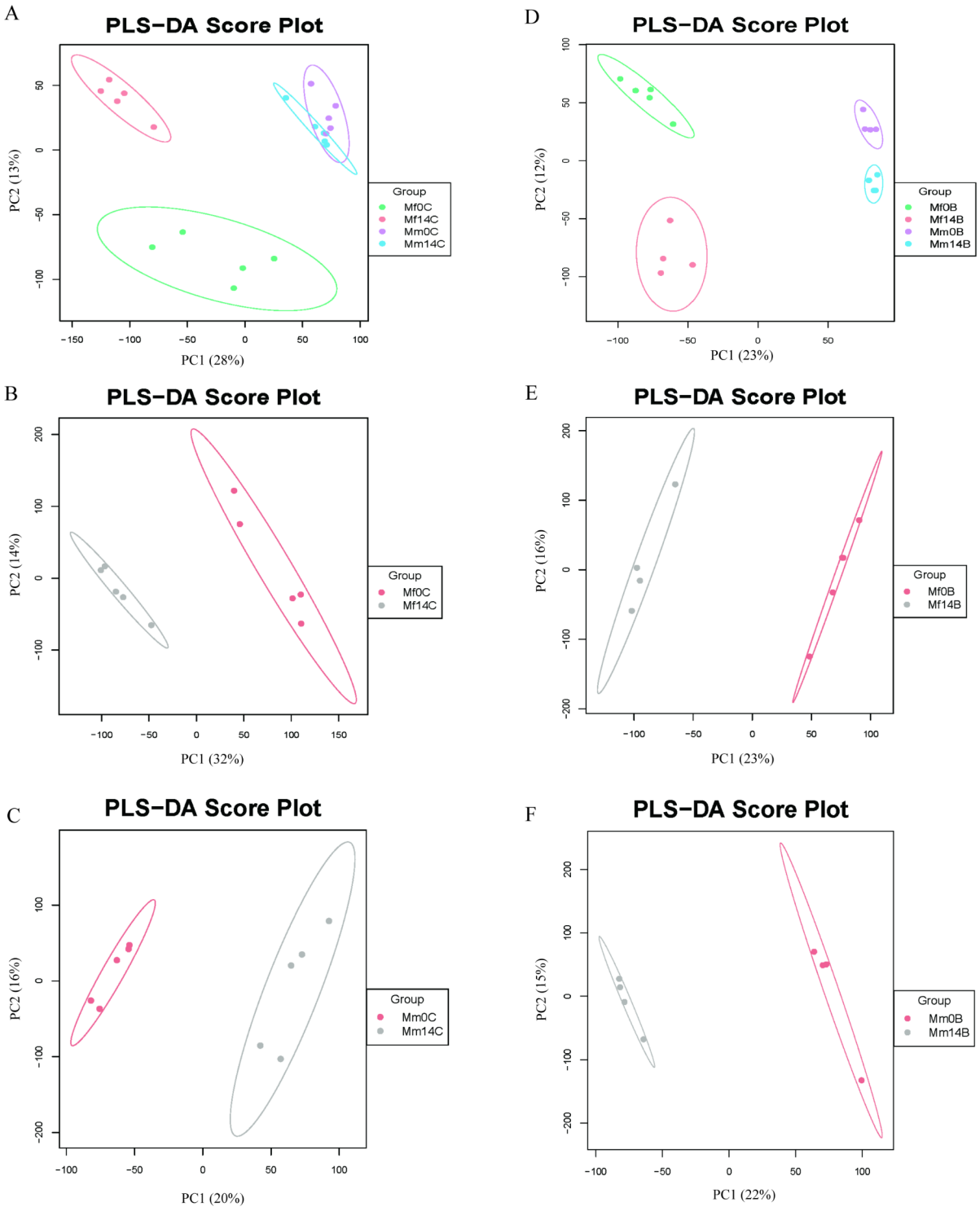

Fig. 2. PLS-DA of M. fortis and ICR mice infected with or without S. japonicum at different time points. Each point represents an individual. (**A**) Colon aqueous extract samples from infected *M. fortis* and infected ICR mice with or without *S. japonicum*. (**B**) Colon aqueous extract samples of infected and uninfected *M. fortis*. (**C**) Colon aqueous extract samples of infected and uninfected ICR mice. (**D**) Serum samples of infected *M. fortis* and infected ICR mice with or without *S. japonicum*. (**E**) Serum samples of infected and uninfected *M. fortis*. (**F**) Serum samples of infected and uninfected ICR mice.

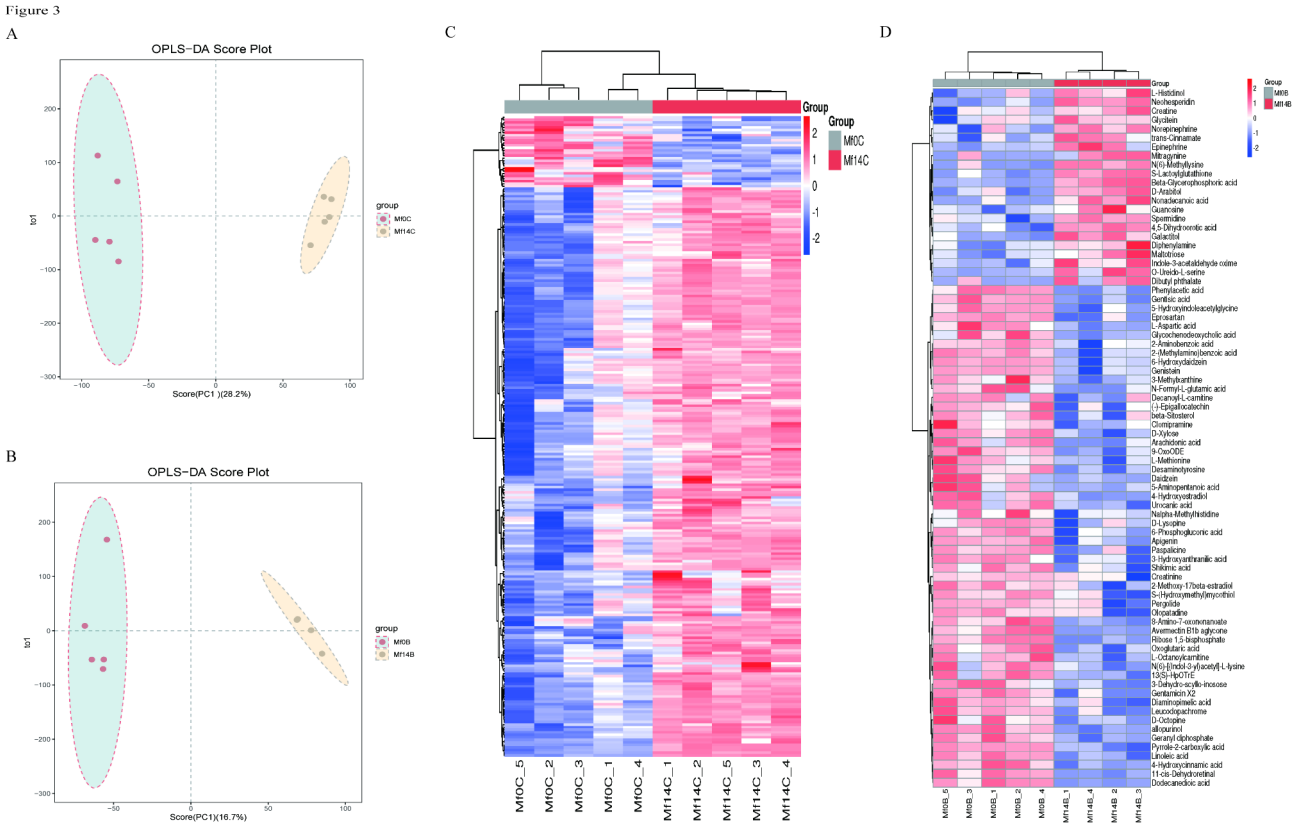

Fig. 3. OPLS-DA combined with covariance and correlation loading profile indicating variable importance in M. fortis. Each point represents a variable. (**A**) Colon aqueous extracts of infected and uninfected *M. fortis*. (**B**) Serum samples of infected and uninfected *M. fortis*. (**C**) Heatmap of the differential colon aqueous extract metabolites between infected and uninfected *M. fortis*. (**D**) Heatmap of the differentially abundant metabolites in serum samples from infected and uninfected *M. fortis*.

"benzene and substituted derivatives" was the most enriched term for the differentially abundant metabolites of *M. fortis* after infection (Fig. 6F).

Pathway enrichment analysis of colon aqueous extracts and serum metabolic profiles

MetaboAnalyst (MESA) was used for the metabolic pathway analysis of the biological roles of the above differentially expressed metabolites. For colon aqueous extract samples, pathway analysis revealed that ABC transporters, biosynthesis of amino acids, taste transduction, phosphotransferase system and alcoholism were significantly enriched between the infected and uninfected *M. fortis* (Fig. 7A). And the tyrosine metabolism, cocaine addiction, amphetamine addiction and alcoholism pathways were significantly enriched between ICR mice with or without infection (Fig. 7B). In addition, arachidonic acid metabolism, serotonergic synapses and biosynthesis of amino acids pathways were significantly enriched between uninfected *M. fortis* and ICR mice (Fig. 7C); and the pathways ABC transporters and central carbon metabolism in cancer were significantly enriched between infected *M. fortis* and ICR mice with *S. japonicum* at two weeks (Fig. 7D). Particularly, the enriched metabolic pathways based on the specific differentially metabolites in *M. fortis* infected with *S. japonicum* at two weeks revealed that central carbon metabolism in cancer, cocaine addiction, and aminobenzoate degradation were significantly enriched (Fig. 7E).

For serum samples, the enriched serum metabolic pathways, including histidine metabolism, biosynthesis of plant secondary metabolites, biosynthesis of plant hormones and biosynthesis of phenylpropanoids and arginine and proline metabolism were enriched between the infected and uninfected *M. fortis* (Fig. 8A). And the ABC transporters, neuroactive ligand-receptor interaction, biosynthesis of plant secondary metabolites, phenylalanine metabolism, linoleic acid metabolism pathways were enriched between ICR mice with or without infection (Fig. 8B). Moreover, pathways lysine degradation, biosynthesis of amino acids, ABC transporters, taste transduction, and bile secretion were significantly enriched between uninfected *M. fortis* and ICR mice (Fig. 8C); and the pathways ABC transporters, biosynthesis of plant secondary metabolites and bile secretion were significantly enriched between infected *M. fortis* and ICR mice (Fig. 8D). Indeed, the enriched pathways in *M. fortis* after infection based on the serum-specific differentially abundant metabolites were ABC transporters, phenylalanine metabolism, neuroactive ligand-receptor interaction, phenylpropanoid biosynthesis, and cysteine and methionine metabolism (Fig. 8E).

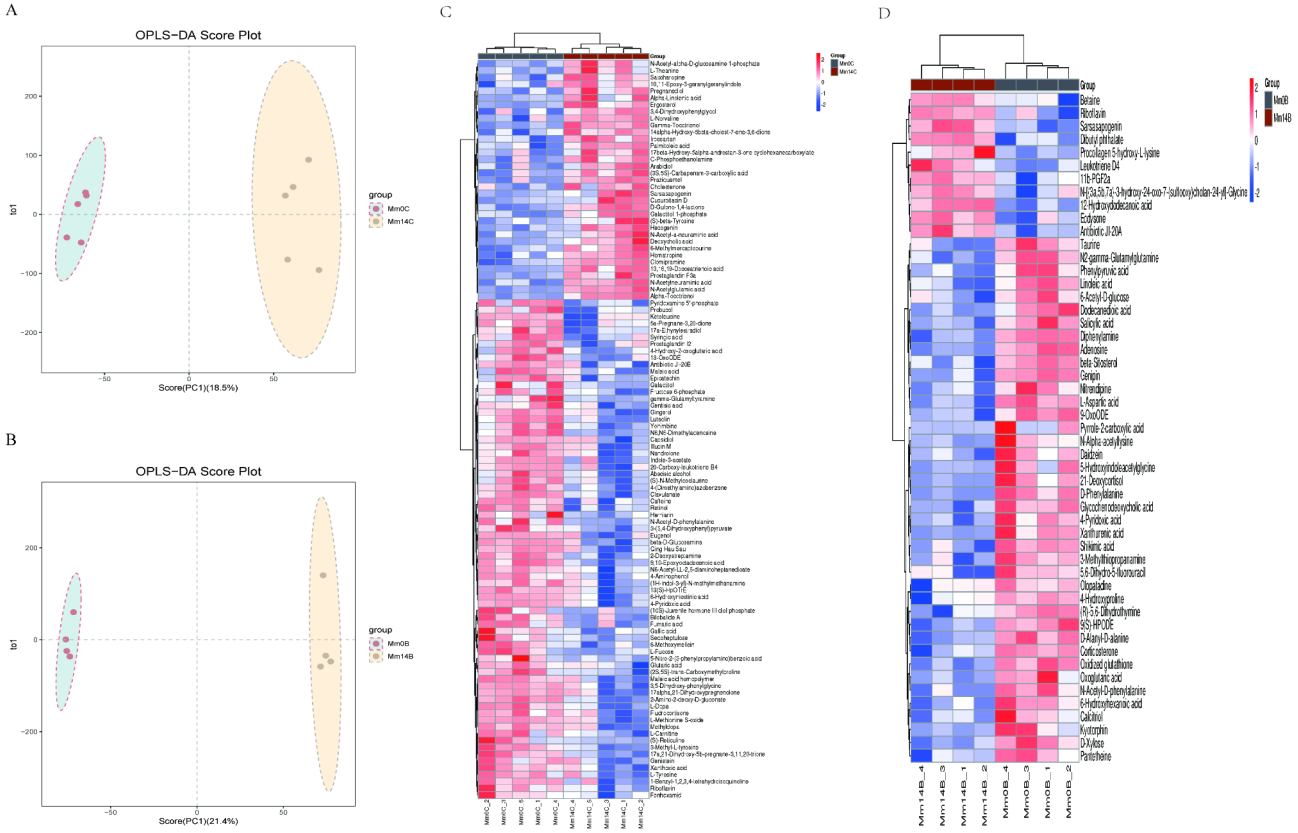

Fig. 4. OPLS-DA combined with covariance and correlation loading profile indicating variable importance in ICR mice. Each point represents a variable. (**A**) Colon aqueous extracts of infected and uninfected ICR mice. (**B**) Serum samples of infected and uninfected ICR mice. (**C**) Hafter infection (194 upregulated and 38 downregulatedeatmap of the differential colon aqueous extract metabolites between infected and uninfected ICR mice. (**D**) Heatmap of the differentially abundant metabolites in serum samples from infected and uninfected ICR mice.

Discussion

In this study, we described the metabolic profiles of colon aqueous extracts and serum in *M. fortis* and ICR mice with or without *S. japonicum* infection using untargeted UPLC-MS/MS-based high-resolution metabolomics analysis. And a series of differentially abundant metabolites were detected in *M. fortis* and ICR mice with or without infection. A summary of the enriched metabolic pathways based on the differential metabolites of *M. fortis* and ICR mice with or without *S. japonicum* infection revealed that the significantly differential metabolites were predominantly enriched in lipid metabolism, amino acid metabolism, bile secretion, and central carbon metabolism in cancer.

Lipids are highly biologically active metabolites that are involved in signaling and immune response modulation and evasion, communication, and the development of inflammatory processes[33]. Previous studies have reported that *S. japonicum* infection induces the reprogramming of lipid metabolism, promotes the expression of genes involved in lipid metabolism in the colon of BALB/c mice, and regulates glycolipid metabolism in the liver of BALB/c mice[34,35]. And the altered lipid metabolism might be a key modulator of host-parasite interactions via mediating the immune responses[36]. Consistent with the previous studies, we also found that lipid metabolism was disrupted after *S. japonicum* infection in *M. fortis* and ICR mice, and that might be related with the host-parasite interactions. For example, fatty acids are essential for *Schistosoma mansoni* egg production, and interference with lipid metabolism affects egg production[37]. During the chronic phase of schistosome infection in mice, proteins associated with the fatty acid cycle are markedly downregulated[38]. Nevertheless, our results revealed that fatty acids were significantly abundant in *M. fortis*. Odd-numbered long-chain fatty acids, nonadecanoic acid (Supplementary Table 9) was the specific and predominant metabolites detected in infected *M. fortis* (FC = 90.91), which might be mainly related to alterations in the gut microbiota[39]. These results implied further confirmation of the disturbed gut microbiome by schistosome infection in *M. fortis* is meaningful. The abundance of alpha-linolenic acid (Supplementary Table 1) in infected *M. fortis* was more than seven-fold greater than that in uninfected *M. fortis*, which is an essential fatty acid that plays important roles in anti-inflammatory, anticancer, antioxidant, and regulation of intestinal flora properties[40]. 5,6-DHET (Supplementary Table 1), a stable metabolite of acachidonic acid was also specifically enriched in *M. fortis*. As we known, acachidonic acid is a safe and effective schistosomicide in mice and hamsters infected with *S. mansoni* and *S. hematobium*[41]. Arachidonic acid metabolism, which is closely related to different inflammatory

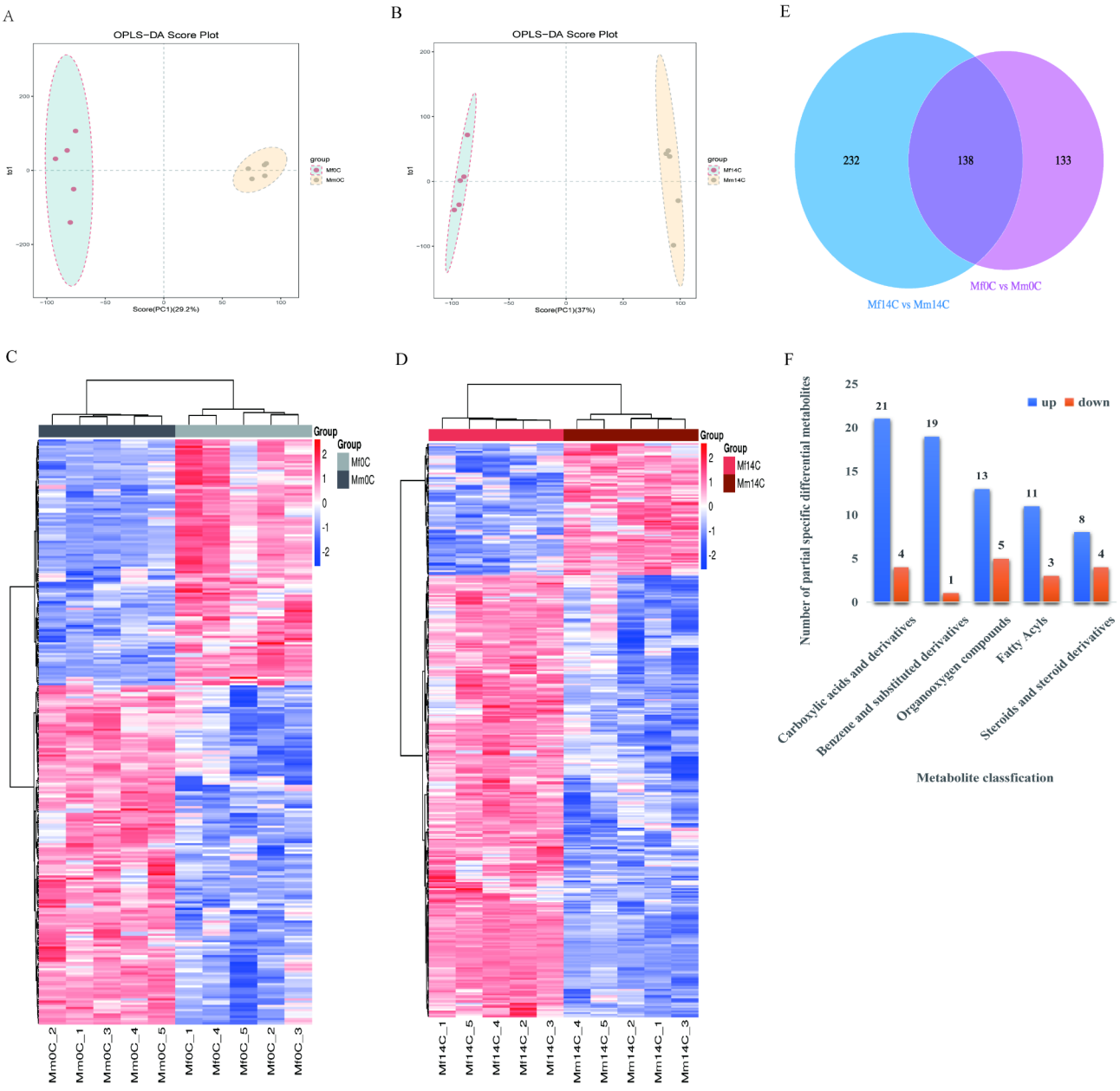

Fig. 5. OPLS-DA of colon aqueous extract samples combined with covariance and the correlation loading profile indicates variable importance between M. fortis and ICR Mice. Each point represents a variable. (**A**) Concerning uninfected *M. fortis* and uninfected ICR mice. (**B**) Concerning infected *M. fortis* and infected ICR mice at two weeks. (**C**) Heatmap of the differential colon aqueous extract metabolites between uninfected *M. fortis* and uninfected ICR mice. (**D**) Heatmap of the differential colon aqueous extract metabolites between *M. fortis* and ICR mice infected with *S. japonicum* at two weeks. (**E**) Venn diagram showing significantly different metabolic responses to *S. japonicum* infection between *M. fortis* and ICR mice. (**F**) Enriched metabolite terms of *M. fortis*-specific differential colon aqueous extract metabolites between *M. fortis* and ICR mice after *S. japonicum* infection.

responses, oxidative stress, and apoptosis[42]. Recent studies revealed that arachidonic acid metabolism was the most prominent pathway involved in the schistosomicidal effects of praziquantel (PZQ) exposure and might be a possible target in the parasiticidal effects of PZQ against *Schistosoma mekongi*[43].

Bile protects organisms from enteric infections by excreting immune globulin A (IgA) and inflammatory cytokines and stimulating the innate immune system in the intestine, and bile is an essential component of the cholehepatic and enterohepatic circulation[44]. Schistosome infections affect the bile secretory apparatus. It has been reported that chronic schistosome infections cause significant changes in the biliary proteome that may produce physiological alterations and affect the therapeutic effects of drugs when administered to human patients and animals with schistosomiasis[45]. Bile acid homeostasis disruption promotes liver injury induced

Figure 6

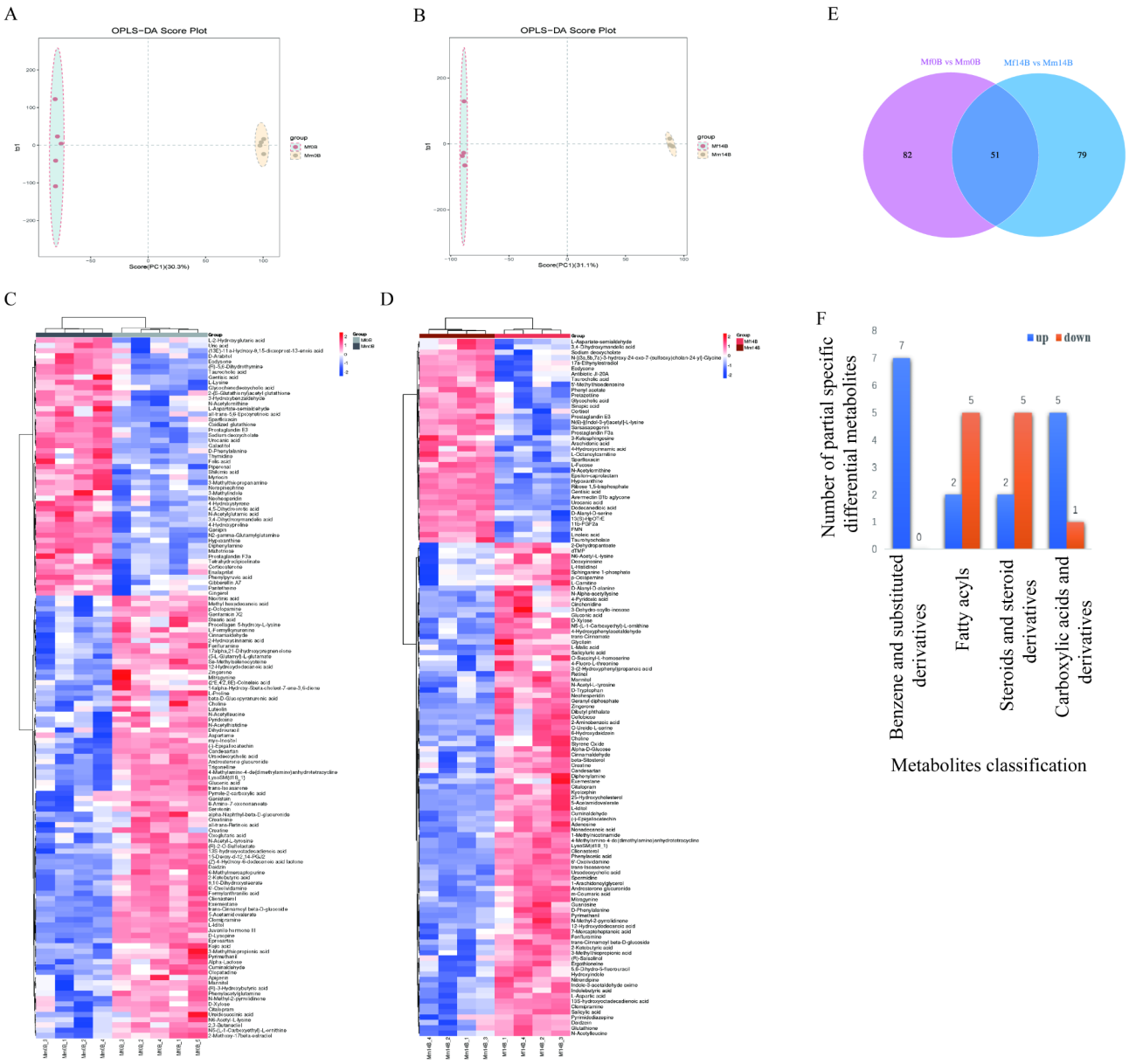

Fig. 6. OPLS-DA of serum samples combined with covariance and correlation loading profile indicating variable importance between M. fortis and ICR Mice. Each point represents a variable. (**A**) Concerning uninfected *M. fortis* and uninfected ICR mice. (**B**) Concerning infected *M. fortis* and infected ICR mice at two weeks. (**C**) Heatmap of the differential serum metabolites between uninfected *M. fortis* and uninfected ICR mice. (**D**) Heatmap of the differential serum metabolites between *M. fortis* and ICR mice infected with *S. japonicum* at two weeks. (**E**) Venn diagram showing significantly different metabolic responses to *S. japonicum* infection between *M. fortis* and ICR mice. (**F**) Enriched metabolite terms of *M. fortis*-specific differential serum metabolites between *M. fortis* and ICR mice after *S. japonicum* infection.

by *S. japonicum* infection in mice[46]. In this study, we found that the bile secretion pathway was enriched in infected *M. fortis*, such as glycocholic acid, was one of the major bile acids and identified as naturally derived anti-inflammatory agent[47]. The abundance of glycocholic acid (Supplementary Table 9) specifically increased in the colon aqueous extracts of infected *M. fortis*. But the glycochenodeoxycholic acid (Supplementary Table 4), a component of bile acid, was significantly decreased in infected ICR mice. Combined with the previous studies that glycocholic acid is associated with schistosomiasis and schistosomiasis-associated carcinogenesis[48]. Thus, the abundance of glycocholic acid was significantly higher in the infected *M. fortis* might activate the immune response of *M. fortis* to resist *S. japonicum* infection.

Another important consequence of liver injury caused by *S. japonicum* infection is the disturbance of amino acid metabolism. Previous studies revealed that the levels of branched-chain amino acids, including valine,

Figure 7

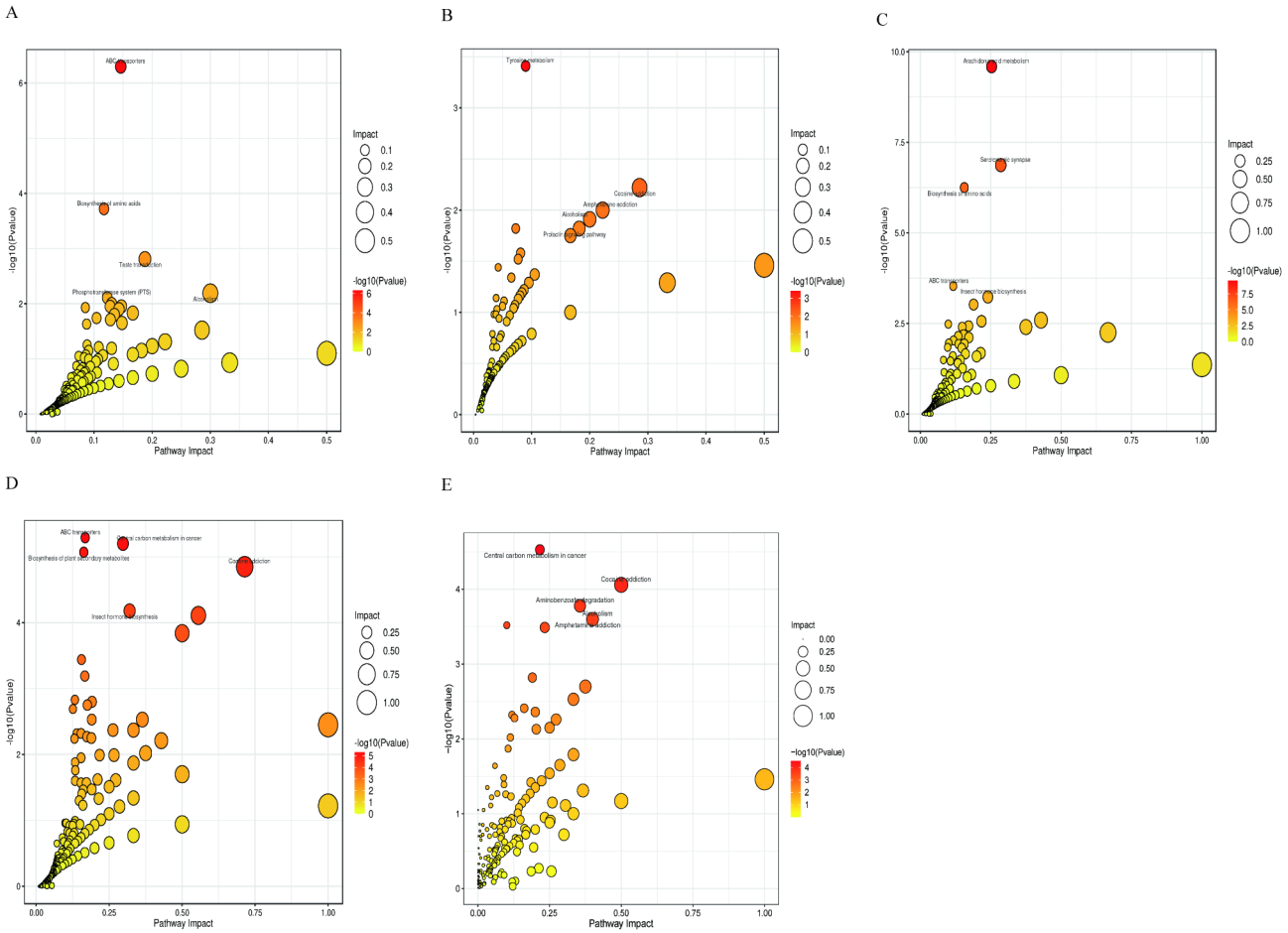

Fig. 7. Maps of the aberrant metabolic pathways associated with the significantly differentially expressed metabolites in the colon aqueous extracts of different groups. The plots show the matched pathways depicted according to the *P* value from pathway enrichment analysis and pathway impact score from pathway topology analysis. In addition, colors varying from yellow to red indicate that the metabolites are present at different levels of significance. (**A**) The enriched metabolic pathways related to specific differentially abundant metabolites in the colon aqueous extracts of *M. fortis* infected with *or without S. japonicum*. (**B**) The enriched metabolic pathways related to specific differentially abundant metabolites in the colon aqueous extracts of ICR mice infected with or without *S. japonicum*. (**C**) The enriched metabolic pathways based on differential colon aqueous extract metabolites between uninfected *M. fortis* and uninfected ICR mice. (**D**) The enriched metabolic pathways based on differential colon aqueous extract metabolites between infected *M. fortis* and infected ICR mice. (**E**) The enriched metabolic pathways based on the specific differentially metabolites in colon aqueous extract of *M. fortis* infected with *S. japonicum* at two weeks.

leucine, and isoleucine, were significantly greater in the liver of *M. fortis* than in that of C57BL/6 mice, and the elevated expression of these metabolites and pathways may promote the phagocytic function of neutrophils and natural killer cell activity and may be related to the resistance mechanism of *M. fortis* against *S. japonicum*[10]. Similarly, our findings regarding amino acid metabolism and amino acid biosynthesis were particularly enriched in *M. fortis*. Glutathione, was the primary cellular antioxidant that buffers reactive oxygen species and exhibited antifungal activity[49]. Recent reports have found that glutathione plays an important role in the fecundity of *S. japonicum*, specifically in egg formation[50]. Therefore, the increasing of glutathione (Supplementary Table 10) could inhibit the development of *S. japonicum* in *M. fortis*. In addition, phenylalanine metabolism and histidine metabolism were also more enriched in infected *M. fortis*, which is consistent with previous studies[51]. Phenylalanine and histidine regulate immune, metabolic responses, and are related with disturbances in gut microbial ecology. Moreover, histidine is an energy source and critical immune modulator involved in parasite persistence within the invertebrate host. Herein, the disturbed phenylalanine metabolism and histidine metabolism in our study may suggest the gut microbiome and immune response were disturbed in *M. fortis* after *S. japonicum* infection, and this finding is consistent with our previous studies[19].

Mammalian ABC transporters influence immune functions, such as cytokine production, Th1 activation, and T-cell migration. It has been reported that ABC transporters may be associated with the development and maintenance of drug resistance in schistosomes, and the disruption of schistosome ABC transporter function

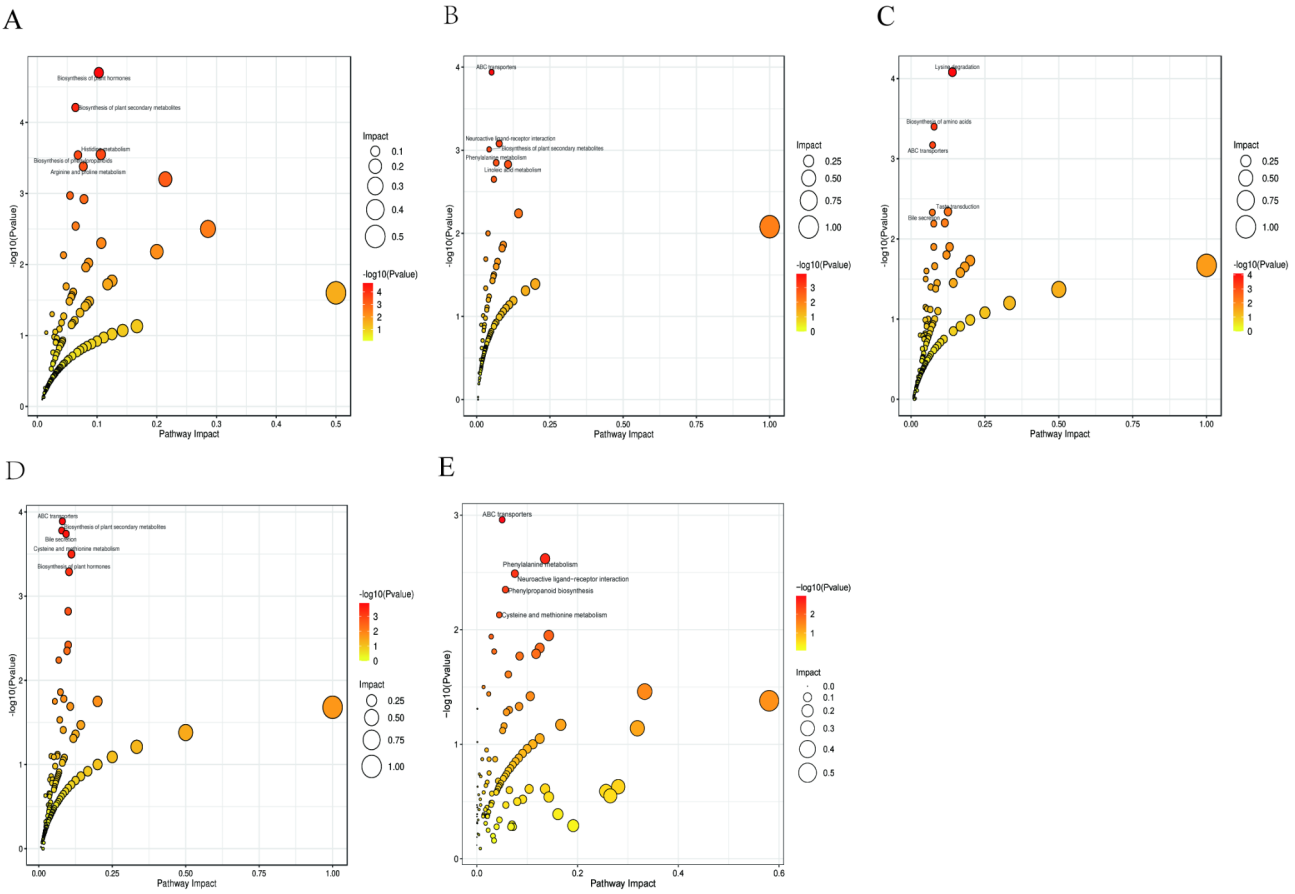

Fig. 8. Maps of the aberrant metabolic pathways based on the significantly differential serum metabolites of different groups. (**A**) The enriched metabolic pathways related to specific differentially abundant metabolites in the serum of *M. fortis* infected with *or without S. japonicum*. (**B**) The enriched metabolic pathways related to specific differentially abundant metabolites in the serum of ICR mice infected with or without *S. japonicum*. (**C**) The enriched metabolic pathways based on differential serum metabolites between uninfected *M. fortis* and uninfected ICR mice. (**D**) The enriched metabolic pathways based on differential serum metabolites between infected *M. fortis* and infected ICR mice. (**E**) The enriched metabolic pathways based on the specific differentially metabolites in serum of *M. fortis* infected with *S. japonicum* at two weeks.

can potentiate the antischistosomal activity of praziquantel (PZQ) against adult worms in culture[52]. In our study, a series of differentially abundant metabolites, including cellobiose (Supplementary Table 10), D-fructose (Supplementary Table 1), and biotin (Supplementary Table 9) were involved in ABC transporters, and the abundances of these metabolites were significantly greater in infected *M. fortis* than infected ICR mice. These results indicated that ABC transporters might evoke host immune responses against *S. japonicum*, but need more experiments to explore.

Some metabolites, such as N-Acetylneuraminic acid (Supplementary Table 1), 13,16,19-Docosatrienoic acid (Supplementary Table 5), (3 S,5 S)-Carbapenam-3-carboxylic acid (Supplementary Table 1) were enriched both in *M. fortis* and ICR mice, indicated these metabolites could be used as markers of schistosome infection. In addition, there is also a series of metabolites with the significant changes in abundance (> 30-fold increases) specially in infected *M. fortis*, including 2-Aminobenzoic acid (Supplementary Table 10), spermidine (Supplementary Table 10), hesperetin (Supplementary Tables 1 and 9), neohesperidin (Supplementary Table 2) and S-lactoylglutathione (Supplementary Table 2). To our knowledge, the 2-Aminobenzoic acid derivatives serve as the inducers of apoptosis, inhibitors of mitogen activated protein kinase pathway, and exhibit interesting antimicrobial, antiviral and insecticidal properties[53]. Therefore, the significantly enriched 2-Aminobenzoic acid in infected *M. fortis* may provide important insights into the mechanism underlying *M. fortis* against *S. japonicum* infection. Spermidine (Supplementary Table 10), a natural polyamine ubiquitously found in organisms, exhibits anti-inflammatory properties and induce autophagy[54]. 6-hydroxydaidzein (Supplementary Table 10) was effective antioxidant[55]. Neohesperidin and hesperetin are citrus flavonoids from the flavanones subclass that possesses various pharmacological properties, including anti-inflammatory, anti-oxidative, anti-apoptosis, and anti-tumor potentials[56,57]. Although the reports about that these metabolites are related with the development of *S. japonicum* is limited now, these results may provide important insights into the mechanism

underlying host-parasite interactions during infection. Furthermore, these metabolites might be used to map on the mechanism involved in the process of *M. fortis* against *S. japonicum* infection.

In summary, we first detected the colon aqueous extracts and serum metabolic profiles between *M. fortis* and ICR mice before and after *S. japonicum* infection and identified a series of differential metabolites in this study. These differential metabolites might participate in affecting the growth and development of schistosome in *M. fortis* and provide insight into the potential metabolic processes and the mechanism underlying the effects of *M. fortis* on schistosome infection. However, no experiments have shown that these metabolites are directly involved in *M. fortis* resistance to schistosomiasis infection in our study. Therefore, we also speculated the metabolite profile differences might come from physiological differences of the different species. In the future, additional experiments to explore the role of these metabolites in *M. fortis* with *S. japonicum* infection are necessary.

Conclusion

In this study, we demonstrated that the metabolites were significantly altered in *M. fortis* infected with *S. japonicum* infection and associated with the time course of *S. japonicum* infection. Compared with ICR mice, nonadecanoic acid, hesperetin, glycocholic acid, 2-Aminobenzoic acid, 6-hydroxydaidzein and spermidine were significantly and specifically increased in *M. fortis* infected with *S. japonicum* for two weeks, when the development of *S. japonicum* in *M. fortis* is arrested and gradually become atrophied. Additionally, the enriched metabolic pathways analyzed between *M. fortis* and ICR mice revealed that the significantly differential metabolites were predominantly enriched in lipid metabolism, amino acid metabolism, bile secretion, ABC transporters and central carbon metabolism in cancer pathways. As a result, our findings might reveal a novel understanding of the resistance mechanisms during schistosomiasis infection in *M. fortis* regarding aspects of the metabolites and facilitated the discovery of promising targets for early diagnosis and anti-schistosome drugs.

Data availability

Data is provided within the manuscript or supplementary information files.

Received: 25 July 2024; Accepted: 18 February 2025
Published online: 28 February 2025

References

1. Verjee, M. A. & Schistosomiasis Still a cause of significant morbidity and mortality. *Res. Rep. Trop. Med.* **10**, 153–163. https://doi.org/10.2147/RRTM.S204345 (2019).
2. Hambrook, J. R. & Hanington, P. C. Immune evasion strategies of schistosomes. *Front. Immunol.* **11**, 624178. https://doi.org/10.3389/fimmu.2020.624178 (2020).
3. Gryseels, B., Polman, K., Clerinx, J. & Kestens, L. Human schistosomiasis. *Lancet* **368**, 1106–1118. https://doi.org/10.1016/S0140-6736(06)69440-3 (2006).
4. Liu, W. Epigenetics in schistosomes: what we know and what we need know. *Front. Cell. Infect. Microbiol.* **6**, 149. https://doi.org/10.3389/fcimb.2016.00149 (2016).
5. McManus, D. P. et al. Schistosomiasis-from immunopathology to vaccines. *Semin Immunopathol.* **42**, 355–371. https://doi.org/10.1007/s00281-020-00789-x (2020).
6. Acharya, S., Da'dara, A. A. & Skelly, P. J. Schistosome immunomodulators. *PLoS Pathog.* **17**, e1010064. https://doi.org/10.1371/journal.ppat.1010064 (2021).
7. Hu, Q. et al. De Novo assembly and transcriptome characterization: Novel insights into the mechanisms of primary ovarian cancer in microtus fortis. *Mol. Med. Rep.* **25**, 64. https://doi.org/10.3892/mmr.2021.12580 (2022).
8. Shen, J. et al. Macrophage-mediated trogocytosis contributes to destroying human schistosomes in a non-susceptible rodent host, Microtus fortis. *Cell. Discov.* **9**, 101. https://doi.org/10.1038/s41421-023-00603-6 (2023).
9. Shen, J., Xiang, S., Peng, M., Zhou, Z. & Wu, Z. Mechanisms of resistance to Schistosoma Japonicum infection in Microtus Fortis, the natural Non-permissive host. *Front. Microbiol.* **11**, 2092. https://doi.org/10.3389/fmicb.2020.02092 (2020).
10. Hu, Y., Sun, L., Yuan, Z., Xu, Y. & Cao, J. High throughput data analyses of the immune characteristics of Microtus fortis infected with Schistosoma Japonicum. *Sci. Rep.* **7**, 11311. https://doi.org/10.1038/s41598-017-11532-2 (2017).
11. Hou, N. et al. Novel hepatic schistosomula antigens as promising targets for immunodiagnosis and Immunoprotection of schistosomiasis Japonica. *J. Infect. Dis.* **225**, 1991–2001. https://doi.org/10.1093/infdis/jiac077 (2022).
12. Li, H. et al. Genome assembly and transcriptome analysis provide insights into the antischistosome mechanism of Microtus fortis. *J. Genet. Genomics*. **47**, 743–755. https://doi.org/10.1016/j.jgg.2020.11.009 (2020).
13. Xiong, D. et al. Transcriptional profiling of Microtus fortis responses to S. japonicum: New sight into Mf-Hsp90α resistance mechanism. *Parasite Immunol.* **43**, e12842. https://doi.org/10.1111/pim.12842 (2021).
14. Bauermeister, A., Mannochio-Russo, H., Costa-Lotufo, L. V., Jarmusch, A. K. & Dorrestein, P. C. Mass spectrometry-based metabolomics in Microbiome investigations. *Nat. Rev. Microbiol.* **20**, 143–160. https://doi.org/10.1038/s41579-021-00621-9 (2022).
15. Vincent, I. M. & Barrett, M. P. Metabolomic-based strategies for anti-parasite drug discovery. *J. Biomol. Screen.* **20**, 44–55. https://doi.org/10.1177/1087057114551519 (2015).
16. Johnson, C. H., Ivanisevic, J. & Siuzdak, G. Metabolomics: Beyond biomarkers and towards mechanisms. *Nat. Rev. Mol. Cell. Biol.* **17**, 451–459. https://doi.org/10.1038/nrm.2016.25 (2016).
17. Huang, Y. et al. UHPLC-MS-Based metabolomics analysis reveals the process of schistosomiasis in mice. *Front. Microbiol.* **11**, 1517. https://doi.org/10.3389/fmicb.2020.01517 (2020).
18. Hong, A., Umar, A., Chen, H., Yu, Z. & Huang, J. Advances in the study of the interaction between schistosome infections and the host's intestinal microorganisms. *Parasit. Vectors*. **17**, 185. https://doi.org/10.1186/s13071-024-06245-1 (2024).
19. Zhang, D. et al. A longitudinal study reveals the alterations of the Microtus fortis colonic microbiota during the natural resistance to Schistosoma Japonicum infection. *Exp. Parasitol.* **219**, 108030. https://doi.org/10.1016/j.exppara.2020.108030 (2020).
20. Hu, Y. et al. De Novo assembly and transcriptome characterization: Novel insights into the natural resistance mechanisms of Microtus fortis against Schistosoma Japonicum. *BMC Genom.* **15**, 417. https://doi.org/10.1186/1471-2164-15-417 (2014).
21. Liu, R. et al. Comparative serum metabolomics between SCID mice and BALB/c mice with or without Schistosoma Japonicum infection: Clues to the abnormal growth and development of schistosome in SCID mice. *Acta Trop.* **200**, 105186. https://doi.org/10.1016/j.actatropica.2019.105186 (2019).

22. Turroni, S. et al. Fecal metabolome of the Hadza hunter-gatherers: A host-microbiome integrative view. *Sci. Rep.* **6**, 32826. https://doi.org/10.1038/srep32826 (2016).
23. Hu, Y. et al. Alterations of gut Microbiome and metabolite profiling in mice infected by Schistosoma Japonicum. *Front. Immunol.* **11**, 569727. https://doi.org/10.3389/fimmu.2020.569727 (2020).
24. Smith, C. A., Want, E. J., O'Maille, G., Abagyan, R. & Siuzdak, G. XCMS: processing mass spectrometry data for metabolite profiling using nonlinear peak alignment, matching, and identification. *Anal. Chem.* **78**, 779–787. https://doi.org/10.1021/ac051437y (2006).
25. Wishart, D. S. et al. HMDB 5.0: The human metabolome database for 2022. *Nucleic Acids Res.* **50**, D622–d631. https://doi.org/10.1093/nar/gkab1062 (2022).
26. Horai, H. et al. MassBank: A public repository for sharing mass spectral data for life sciences. *J. Mass. Spectrom.* **45**, 703–714. https://doi.org/10.1002/jms.1777 (2010).
27. Sud, M. et al. LIPID MAPS structure database. *Nucleic Acids Res. 35*. **LMSD**, D527–532. https://doi.org/10.1093/nar/gkl838 (2007).
28. Abdelrazig, S. et al. Metabolic characterisation of Magnetospirillum gryphiswaldense MSR-1 using LC-MS-based metabolite profiling. *RSC Adv.* **10**, 32548–32560. https://doi.org/10.1039/d0ra05326k (2020).
29. Kanehisa, M. & Goto, S. KEGG: Kyoto encyclopedia of genes and genomes. *Nucleic Acids Res.* **28**, 27–30. https://doi.org/10.1093/nar/28.1.27 (2000).
30. Kanehisa, M. et al. KEGG: Biological systems database as a model of the real world. *Nucleic Acids Res.* **53**, D672–D677. https://doi.org/10.1093/nar/gkae909 (2025).
31. Gagnebin, Y. et al. Metabolomic analysis of urine samples by UHPLC-QTOF-MS: Impact of normalization strategies. *Anal. Chim. Acta*. **955**, 27–35. https://doi.org/10.1016/j.aca.2016.12.029 (2017).
32. Xia, J. & Wishart, D. S. Web-based inference of biological patterns, functions and pathways from metabolomic data using metaboanalyst. *Nat. Protoc.* **6**, 743–760. https://doi.org/10.1038/nprot.2011.319 (2011).
33. Calder, P. C. Polyunsaturated fatty acids, inflammation, and immunity. *Lipids* **36**, 1007–1024. https://doi.org/10.1007/s11745-001-0812-7 (2001).
34. Yang, X. et al. Schistosoma Japonicum infection leads to the reprogramming of glucose and lipid metabolism in the Colon of mice. *Front. Veterinary Sci.* **8** https://doi.org/10.3389/fvets.2021.645807 (2021).
35. Gonçalves-Silva, G. et al. Profiling the serum proteome during Schistosoma mansoni infection in the BALB/c mice: A focus on the altered lipid metabolism as a key modulator of host-parasite interactions. *Front. Immunol.* **13**, 955049. https://doi.org/10.3389/fimmu.2022.955049 (2022).
36. Xin-yu, Q. et al. The metabolic reprogramming profiles in the liver fibrosis of mice infected with Schistosoma Japonicum. *Inflammation* **43**, 731–743. https://doi.org/10.1007/s10753-019-01160-5 (2020).
37. Bexkens, M. L. et al. Schistosoma mansoni does not and cannot oxidise fatty acids, but these are used for biosynthetic purposes instead. *Int. J. Parasitol.* **49**, 647–656. https://doi.org/10.1016/j.ijpara.2019.03.005 (2019).
38. Harvie, M., Jordan, T. W. & La Flamme, A. C. Differential liver protein expression during schistosomiasis. *Infect. Immun.* **75** (2), 736–744. https://doi.org/10.1128/IAI.01048-06 (2007).
39. Lv, L., Du, M. D., Yan, Y. & Jiang, R. Mechanism of the immunomodulatory effect of the combination of live bifidobacterium, Lactobacillus, Enterococcus, and Bacillus on immunocompromised rats. *Front. Immunol.* **12**, 694344. https://doi.org/10.3389/fimmu.2021.694344 (2021).
40. Yuan, Q. et al. The review of alpha-linolenic acid: Sources, metabolism, and Pharmacology. *Phytother. Res.* **36**, 164–188. https://doi.org/10.1002/ptr.7295 (2021).
41. Tallima, H., Hanna, V. S. & El Ridi, R. Arachidonic acid is a safe and efficacious schistosomicide, and an endoschistosomicide in natural and experimental infections, and cysteine peptidase vaccinated hosts. *Front. Immunol.* **11**, 609994. https://doi.org/10.3389/fimmu.2020.609994 (2020).
42. Zhang, C. et al. The role of arachidonic acid metabolism in myocardial Ischemia-Reperfusion injury. *Cell. Biochem. Biophys.* **78**, 255–265. https://doi.org/10.1007/s12013-020-00928-z (2020).
43. Chienwichai, P. et al. Metabolomics reveal alterations in arachidonic acid metabolism in Schistosoma Mekongi after exposure to praziquantel. *PLoS Negl. Trop. Dis.* **15**, e0009706. https://doi.org/10.1371/journal.pntd.0009706 (2021).
44. Trauner, M., Fuchs, C. D., Halilbasic, E. & Paumgartner, G. New therapeutic concepts in bile acid transport and signaling for management of cholestasis. *Hepatology* **65** (4), 1393–1404. https://doi.org/10.1002/hep.28991 (2017).
45. Manivannan, B., Jordan, T. W., Secor, W. E. & La flamme, A. C. Proteomic changes at 8 weeks after infection are associated with chronic liver pathology in experimental schistosomiasis. *J. Proteom.* **75**, 1838–1848. https://doi.org/10.1016/j.jprot.2011.12.025 (2012).
46. Zhang, B. et al. FXR deficiency in hepatocytes disrupts the bile acid homeostasis and inhibits autophagy to promote liver injury in Schistosoma japonicum-infected mice. *PLoS Negl. Trop. Dis.* **16**, e0010651. https://doi.org/10.1371/journal.pntd.0010651 (2022).
47. Ge, X., Ren, H. S. & Zhao, C. L. Taurocholic acid and glycocholic acid inhibit inflammation and activate farnesoid X receptor expression in LPS-stimulated zebrafish and macrophages. *Molecules* **28** (2005). https://doi.org/10.3390/molecules28052005 (2023).
48. Yuan, Z. et al. Glycocholic acid aggravates liver fibrosis by promoting the up-regulation of connective tissue growth factor in hepatocytes. *Cell. Signal.* **101**, 110508. https://doi.org/10.1016/j.cellsig.2022.110508 (2023).
49. Lv, H. et al. Unraveling the potential role of glutathione in multiple forms of cell death in Cancer therapy. *Oxid. Med. Cell. Longev.* **2019** (3150145). https://doi.org/10.1155/2019/3150145 (2019).
50. Tang, C. L., Zhou, H. H., Zhu, Y. W., Huang, J. & Wang, G. B. Glutathione S-transferase influences the fecundity of Schistosoma Japonicum. *Acta Trop.* **191**, 8–12. https://doi.org/10.1016/j.actatropica.2018.12.027 (2019).
51. Kay, G. L. et al. Differences in the faecal Microbiome in Schistosoma haematobium infected children vs. Uninfected children. *PLoS Negl. Trop. Dis.* **9**, e0003861. https://doi.org/10.1371/journal.pntd.0003861 (2015).
52. Davies, S. J. et al. Inhibition or knockdown of ABC transporters enhances susceptibility of adult and juvenile schistosomes to praziquantel. *PLoS Negl. Trop. Dis.* **8** https://doi.org/10.1371/journal.pntd.0003265 (2014).
53. Parteek Prasher, M. S. Medicinal chemistry of anthranilic acid derivatives: A mini review. *Drug Dev. Res.* **82**,, 945–958. https://doi.org/10.1002/ddr.21842 (2021).
54. Hofer, S. J., Bergmann, S. A., Eisenberg, M., Kroemer, T. & Madeo, G. Mechanisms of spermidine-induced autophagy and geroprotection. *Nat. Aging.* **2**, 1112–1129. https://doi.org/10.1038/s43587-022-00322-9 (2022).
55. Kampkötter, A. et al. Isoflavone Daidzein possesses no antioxidant activities in cell-free assays but induces the antioxidant enzyme catalase. *Nutr. Res.* **28**, 620–628. https://doi.org/10.1016/j.nutres.2008.06.002 (2008).
56. Ortiz, A. C. Therapeutic effects of Citrus flavonoids neohesperidin, hesperidin and its Aglycone, Hesperetin on bone health. *Biomolecules* **12**, 626. https://doi.org/10.3390/biom12050626 (2022).
57. Lu, Z. Hesperetin attenuates UVA-induced photodamage in human dermal fibroblast cells. *J. Cosmet. Dermatol.* **21**, 6261–6269. https://doi.org/10.1111/jocd.15230 (2022).

Author contributions

Conceptualization, Zhijun Zhou and Tianqiong He; Methodology, Du Zhang and Jia Shen; Software, Du Zhang; Validation, Yixin Wen and Qian Liu; Data Curation, Junkang Zhou and Wenling Zhi; Writing—Original Draft Preparation, Zhijun Zhou and Tianqiong He; Writing—Review & Editing, Zhijun Zhou and Tianqiong He; Vis-

ualization, Lingxuan OuYang, Yushan Qi, Zikang Zhou, Xin Gao, Fan Li, Zhijie Su; Supervision, Jia Shen; The author(s) read and approved the final manuscript.

Funding
This work was supported by grants from the Changsha major special project of science and technology (kh2301027), natural science foundation of Hunan province (2024JJ5422), natural science foundation of Hunan province (2024JJ6494), key Research and development Program of Hunan Province (2024DK2001).

Declarations

Competing interests
The authors declare no competing interests.

Additional information
Supplementary Information The online version contains supplementary material available at https://doi.org/10.1038/s41598-025-91164-z.

Correspondence and requests for materials should be addressed to Z.Z.

Reprints and permissions information is available at www.nature.com/reprints.

Publisher's note Springer Nature remains neutral with regard to jurisdictional claims in published maps and institutional affiliations.

Open Access This article is licensed under a Creative Commons Attribution-NonCommercial-NoDerivatives 4.0 International License, which permits any non-commercial use, sharing, distribution and reproduction in any medium or format, as long as you give appropriate credit to the original author(s) and the source, provide a link to the Creative Commons licence, and indicate if you modified the licensed material. You do not have permission under this licence to share adapted material derived from this article or parts of it. The images or other third party material in this article are included in the article's Creative Commons licence, unless indicated otherwise in a credit line to the material. If material is not included in the article's Creative Commons licence and your intended use is not permitted by statutory regulation or exceeds the permitted use, you will need to obtain permission directly from the copyright holder. To view a copy of this licence, visit http://creativecommons.org/licenses/by-nc-nd/4.0/.

© The Author(s) 2025